Quantum Chemical Insight into the LiF Interlayer Effects in Organic Electronics: Reactions between Al Atom and LiF Clusters

ARTICLE *in* JOURNAL OF PHYSICAL CHEMISTRY LETTERS · JULY 2015

Impact Factor: 7.46 · DOI: 10.1021/acs.jpclett.5b01182

6 AUTHORS, INCLUDING:

Shui-Xing Wu

Northeast Normal University

22 PUBLICATIONS **317** CITATIONS

SEE PROFILE

Yu-He Kan

Huaiyin Normal University

137 PUBLICATIONS **1,051** CITATIONS

SEE PROFILE

Hai-Bin Li

Northeast Normal University

42 PUBLICATIONS **747** CITATIONS

SEE PROFILE

Yong wu

University of Hawai‘i at Mānoa

38 PUBLICATIONS **441** CITATIONS

SEE PROFILE

THE JOURNAL OF PHYSICAL CHEMISTRY Letters

Letter

pubs.acs.org/JPCL

Quantum Chemical Insight into the LiF Interlayer Effects in Organic Electronics: Reactions between Al Atom and LiF Clusters

Shui-Xing Wu,[†] Yu-He Kan,[‡] Hai-Bin Li,[†] Liang Zhao,[†] Yong Wu,[†] and Zhong-Min Su*,[†]

[†]Institution of Functional Material Chemistry, Department of Chemistry, Northeast Normal University, Changchun 130024, China

[‡]Jiangsu Province Key Laboratory for Chemistry of Low-Dimensional Materials, School of Chemistry and Chemical Engineering, Huaiyin Normal University, Huaian 223300, China

Supporting Information

ABSTRACT: It is well known that the aluminum cathode performs dramatically better when a thin lithium fluoride (LiF) layer inserted in organic electronic devices. The doping effect induced by the librated Li atom via the chemical reactions producing AlF_3 as byproduct was previously proposed as one of possible mechanisms. However, the underlying mechanism discussion is quite complicated and not fully understood so far, although the LiF interlayer is widely used. In this paper, we perform theoretical calculations to consider the reactions between an aluminum atom and distinct LiF clusters. The reaction pathways of the Al−$(LiF)_n$ (n = 2, 4, 16) systems were discovered and the energetics were theoretically evaluated. The release of Li atom and the formation of AlF_3 were found in two different chemical reaction routes. The undissociated Al−$(LiF)_n$ systems have chances to change to some structures with loosely bound electrons. Our findings about the interacted Al−$(LiF)_n$ systems reveal new insights into the LiF interlayer effects in organic electronics applications.

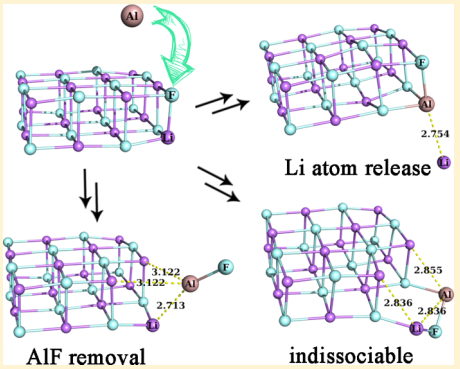

Despite possessing a bright future, organic electronic devices still have some obstacles to overcome before their extensive applications in competitive market products.[1,2] Among these aspects, the issue on charge carrier transfer across the organic layer (OL)/electrode interfaces is of high concern for an efficient organic electronic device.[3−7] To polish the interface electron process across OL/cathode, lithium fluoride (LiF) and other alkali halides (AHs) were introduced into organic light emitting diodes (OLEDs)[8,9] and organic photovoltaic cells (OPVCs)[10,11] as interlayers. The enhancement effect of LiF on device performances has been explained by several mechanisms, mainly including tunneling effect,[12,13] doping effect induced by chemical reactions,[14−16] interface dipole formation,[17−19] and band bending,[20,21] where conflicting views were often presented, and it remains to be fully understood.[22−24]

As for the mechanism based on chemical reactions, the common understanding is the reaction occurring at the ternary interface Al/LiF/tris(8-hydroxyquinoline)-aluminum (Alq_3), that is, Al + 3LiF + 3Alq_3 → AlF_3 + 3$Li^+Alq_3^-$, which was proposed by Mason et al.[15,16] and considered again by Wu et al.[25] The performance enhancements were also elaborated by proposing other types of chemical reactions, such as the reaction occurring between LiF and Alq_3 before Al deposition[26] or the reaction assisted by the possibly present water.[14] Although the chemical reaction model is not valid for all the cases of different interfaces, for example, Al/LiF deposited on poly(9,9-dioctyl-fluorene), MDMO-PPV or PCBM,[27−29] the Li liberation via dissociation of LiF was evidenced even lately.[30−33] Moreover, the optimal LiF thickness was reported as around 0.5 nm,[8,34,35] and considering the incomplete surface coverage of such thin LiF interlayers,[36,37] the nanosized LiF clusters were suggested to be taken into account.[38] The pressure during the deposition process was on the order of 10^{-6} Torr,[9,12] allowing for that Al atoms could be deposited onto the LiF/OL surface one by one.

As the very complicated effects of LiF on the performance enhancements have been manifested for nearly two decades, a more clear understanding is badly required to guide the constructions of better devices. In this regard, we believe it should be very helpful to execute an investigation on the microscopic reaction pathways of the chemical reactions between Al atom and LiF clusters and to evaluate the barrier heights of the discovered reactions. In this study, two small clusters, the rhombic $(LiF)_2$ and the cubic $(LiF)_4$, and one medium-sized cluster 4 × 4 × 2 $(LiF)_{16}$ are adopted as examples, and density functional theory (DFT) methods are employed to explore the reactions between Al atom and the example clusters. We chose the parameter-free hybrid functional PBE0[39] to perform the optimizations for all stationary structures and to characterize the optimized structures as minima or transition states via the calculations of harmonic vibrational frequencies. The Karlsruhe basis set def2-TZVP[40] was used, and the "ma-" kind of diffuse functions were added

Received: June 4, 2015
Accepted: July 14, 2015

DOI: 10.1021/acs.jpclett.5b01182
J. Phys. Chem. Lett. 2015, 6, 2950−2958

due to some involved systems with one singly occupied electron delocalized between the atoms at long interatomic distances.[41] Zero-point energy (ZPE) corrections have been included for the relative energy parameters and the activation energies. The energy parameters for the selected reactions were also calculated using M06[42]/ma-def2-TZVP. The intrinsic reaction coordinate (IRC)[43,44] scans were performed at the PBE0/def2-TZVP level to verify the connections between the stationary points along reaction pathways. The vertical ionization energies (VIEs) were obtained by calculating the differences between the neutral state energies and the cation state ones at neutral geometries. The outer valence Green function (OVGF) approach[45−47] was also employed to produce more accurate VIEs and the vertical electron affinities (VEAs) for cation structures. All these calculations were performed using the Gaussian 09 program suite.[48]

Unlike other alkali fluorides, the vapor phase of LiF contains a significant fraction of dimer.[49,50] The dimer $(LiF)_2$ may exist in the evaporatedly deposited thin interlayer of organic devices. Its global minimum is in a planar rhombic shape.[51] The PBE0 optimized Li−F bond distance and Li−F−Li angle are 1.719 Å and 80.8°, respectively, which are very close to the reported MP2 values 1.724 Å and 79.9°.[52] The structure **2A** was considered as the starting one, and other stationary structures (shown in Figure 1) were searched and connected in the pathways as given in Figure 2.

2A is the most stable minimum, and the energy of formation from its interacting Al atom and $(LiF)_2$ is −32.65 kcal/mol (calculated by PBE0, see reaction 1 in Table 1). Along the reaction pathway **2A** → **2B** → **2C**, there are two step barriers of 9.12 and 10.19 kcal/mol, and **2C** stands higher in energy by 11.25 kcal/mol relative to **2A**. Notably, a weak Al−Li interaction exists in **2C**, where the dissociation (reaction 2 in Table 1) to Li atom and **2C-li** (i.e., the ring structure of $AlLiF_2$) needs to overcome an energy of 10.31 kcal/mol (PBE0). In the subpathway **2B** → **2D**, the transition state (**2TS3**) lies much lower in energy than the transition state (**2TS2**) connecting **2B** and **2C**. **2D** also lies much lower in energy than **2C**, but in **2D**,

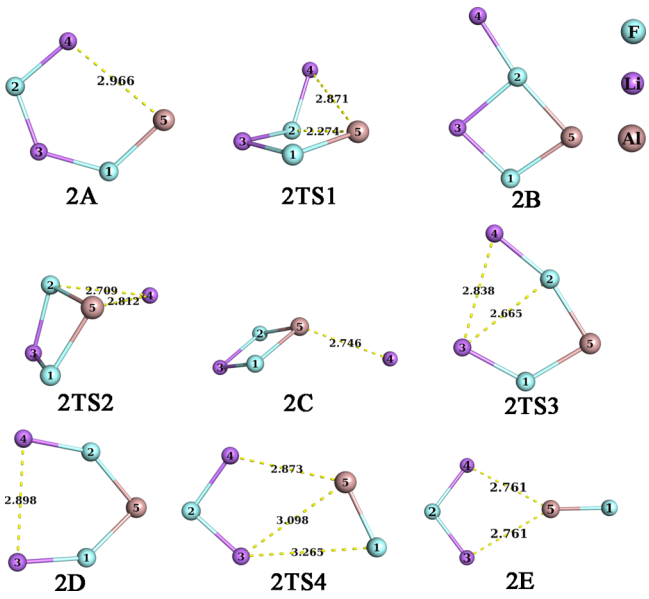

Figure 1. PBE0 optimized stationary structures involved in the Al−$(LiF)_2$ system (labeled interatomic distances in Å).

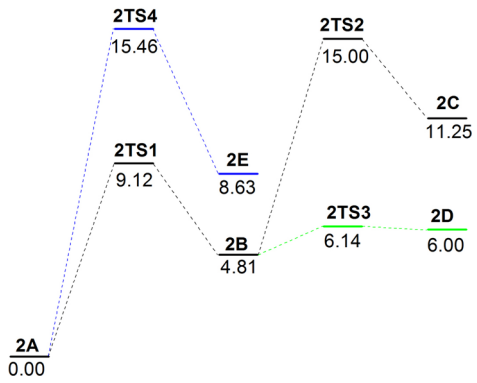

Figure 2. Energy profile for the reactions of the Al−$(LiF)_2$ system, with the labeled ZPE-corrected energies (in kcal/mol, calculated by PBE0) relative to **2A**.

Table 1. Calculated Reaction Energies, Δ*E* in kcal/mol, ZPE-Corrected, for the Al−$(LiF)_2$ System

reaction	PBE0	M06
Al + $(LiF)_2$ → **2A** (1)	−32.65	−31.44
2C → Li + **2C-li** (2)	10.31	8.52
2E → AlF + **2E-alf** (3)	21.78	19.71
Al + $(LiF)_2$ → **2C-li** + Li (4)	−11.09	−12.32
Al + $(LiF)_2$ → **2E-alf** + AlF (5)	−2.24	−1.29

there is no weakly bonded connection, like obviously partible connections in **2C** and **2E**, suggesting no facile dissociation reaction should occur from **2D**. The energy barrier for the process **2A** → **2E** is as high as 15.46 kcal/mol. The dissociation (reaction 3 in Table 1) from **2E** to AlF and **2E-alf** (i.e., Li_2F) needs to overcome an energy of 21.78 kcal/mol (PBE0).

Considering the start from the reaction of Al atom and $(LiF)_2$, we calculated the energies for two reactions (reactions 4 and 5 in Table 1). The replacement reaction [Al + $(LiF)_2$ → **2C-li** + Li] is −11.09 kcal/mol (PBE0) exothermic. The exothermicity of reaction 5 is much smaller, and the reaction energy are predicted as −2.24 and −1.29 kcal/mol by PBE0 and M06, respectively. The M06 values in Table 1 are close to the PBE0 ones, and both should lead to the same conclusions.

Additionaly, in the Al−$(LiF)_2$ system, there is no real minimum structure found with the Al atom tail attached to one F atom. The C_{2v} Al-tail structure (see Figure S2 in the Supporting Information) corresponds to a second order saddle (with two negative frequencies), around which one C_s structure (**2TS5** shown in Figure S2) was found as a transition state, with a barrier of 11.26 kcal/mol, connecting two equivalent conformers of **2A**.

The thickness around 0.5 nm of LiF interlayer is acturally average, and the lattice constant of LiF (rock salt) solid is 4.03 Å. Thus, two monolayers (2 ML) height of LiF islands should be dominant in 0.5 nm-thick LiF interlayer. The cubic 2 × 2 × 2 structure is the smallest rock salt cluster with 2 ML height and is the global minimum of the tetramer $(LiF)_4$.[51−54] The PBE0 optimized Li−F bond distance in the 2 × 2 × 2 $(LiF)_4$ is 1.823 Å, which is very close to the reported MP2 value 1.824 Å.[52] The Al-binding structure **4A** was found as the most stable minimum, and the structures of **4A** and the other searched minima are shown in Figure 3. All the searched minima were verified to be connected in the pathways depicted in Figure 4,

DOI: 10.1021/acs.jpclett.5b01182
J. Phys. Chem. Lett. 2015, 6, 2950−2958

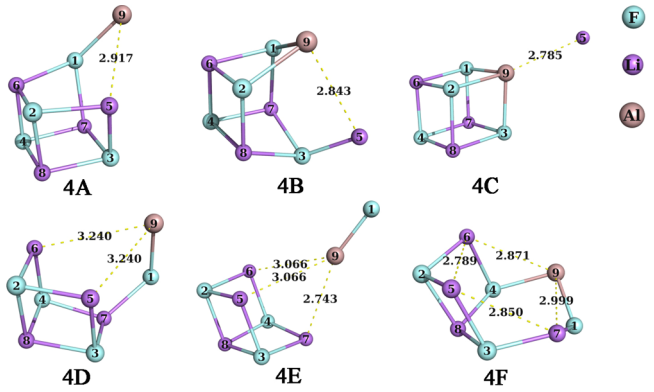

Figure 3. PBE0 optimized minimum structures involved in the Al−$(LiF)_4$ system (labeled interatomic distances in Å).

whereas the structures of the transition states are shown in the Supporting Information.

The energy for the formation of **4A** from its interacting moieties Al atom and 2 × 2 × 2 $(LiF)_4$ was calculated using PBE0 as −22.34 kcal/mol (see reaction 6 in Table 2), which is smaller than the corresponding value (−32.65 kcal/mol) of **2A**. This can be understood by considering that the geometrical changes from 2 × 2 × 2 $(LiF)_4$ to **4A** are significantly constrained in comparison to the ones from the rhombic $(LiF)_2$ to **2A**. Along the pathway **4A** → **4B** → **4C**, the fisrt barrier is 6.01 kcal/mol and the second one is 12.30 kcal/mol. **4C** occupies a position higher than **4A** by 13.28 kcal/mol in the potential energy surface (PES). Due to the weakly bonded Li atom, **4C** can experience a dissociation (reaction 7 in Table 2) to one free Li atom and the remnant moiety **4C-li** when it overcome a binding energy of 10.11 kcal/mol (PBE0). In the pathway **4A** → **4D** → **4E**, there are two energy barriers of 2.95 and 11.57 kcal/mol. From **4E**, the dissociation (reaction 8 in Table 2) to the monomolecular AlF and the remnant moiety **4E-alf** (i.e., Li_4F_3) needs to overcome an energy of 21.21 kcal/mol, similar to reaction 3. In one subpathway the process **4D** → **4F** has an energy barrier of 6.24 kcal/mol. The produced **4F** lies lower than **4C** and **4E** in energy, but no facile dissociation reaction was found from **4F**.

Reactions 9 and 10 listed in Table 2 are for examining the overall processes from the interaction of Al atom with 2 × 2 × 2 $(LiF)_4$ to the dissociated products. Unlike reactions 4 and 5 listed in Table 1, reactions 9 and 10 are endothermic, although

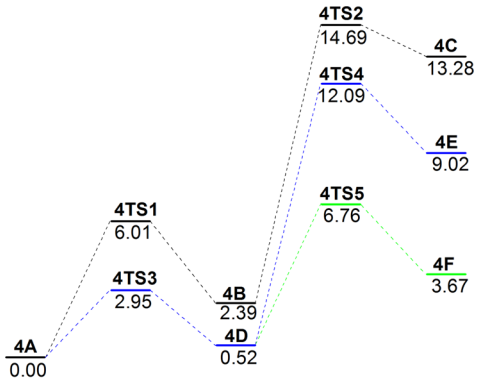

Figure 4. Energy profile for the reactions of the Al−$(LiF)_4$ system, with the labeled ZPE-corrected energies (in kcal/mol, calculated by PBE0) relative to **4A**.

Table 2. Calculated Reaction Energies, Δ*E* in kcal/mol, ZPE-Corrected, for the Al−$(LiF)_4$ System

reaction		PBE0	M06
Al + 2 × 2 × 2$(LiF)_4$ → **4A**	(6)	−22.34	−21.14
4C → Li + **4C-li**	(7)	10.11	9.02
4E → AlF + **4E-alf**	(8)	21.21	20.22
Al + 2 × 2 × 2$(LiF)_4$ → **4C-li** + Li	(9)	1.05	1.36
Al + 2 × 2 × 2$(LiF)_4$ → **4E-alf** + AlF	(10)	7.89	10.82

the endothermicities are small, especially for reactions 9 (1.05 kcal/mol by PBE0). The endothermicities may need to be compensated by some interactions. Again, the same conclusions should be drawn from the two columns of results based on M06 and PBE0, respectively, collected in Table 2.

In addition, unlike the stability of the C_{3v} Li-tail structure of Li_5F_4,[55] the C_{3v} structure of Al$(LiF)_4$ (with Al attached onto one F) needs to experience a Jahn−Teller distortion to the structure (i.e., **4A**) with Al swinging to one edge. Nearby, one C_s structure (**4TS6** shown in Supporting Information Figure S2) was found as a transition state connecting the two equivalent conformers of **4A** with the Al atom swinging to the two adjacent edges, respectively. The transition between the two equivalent conformers has a 3.31 kcal/mol energy barrier. We also found another C_{2v} transition state (**4TS7** shown in Supporting Information Figure S2), with a barrier of 6.84 kcal/mol, connecting the two equivalent conformers of **4A** with the Al atom swinging to the two opposite edges, respectively, in one facet.

To our knowledge, no global minimum structure of $(LiF)_{16}$ has been stated so far. Herein, we focus more attention on the rock salt structure with a low height, to better match the possible cases in the thin LiF interlayer. The 2 × 2 × 2 $(LiF)_4$ structure may also represent the corner state of larger-sized cluster islands, but the surrounding atoms in a larger-sized cluster can change the geometrical relaxations of intermediums or products. Therefore, 4 × 4 × 2 $(LiF)_{16}$ was chosen to consider the size effects, although there may be some other structures at a possibly lower energy level, such as the cage structure of $(LiF)_{16}$ in the manner of $(ZnO)_{16}$.[56] A similar example is the cluster $(LiF)_{12}$, whose cage structure was reported more stable than the slab structure.[57] When Al atom interacts with 4 × 4 × 2 $(LiF)_{16}$, it starts from one corner F atom and forms the structure **16A**, which is the most stable one. All the PBE0 optimized minimum structures in the Al−$(LiF)_{16}$ are shown in Figure 5, and the involved transtion state structures are given in the Supporting Information. All the found stationary points are connected in the pathways shown in Figure 6.

The PBE0 calculated energy for the formation of **16A** from the interacting Al atom and 4 × 4 × 2 $(LiF)_{16}$ is −21.91 kcal/mol (see reaction 11 in Table 3), which is close to the corresponding value of **4A**. As revealed in Figure 6, during the process **16A** → **16B** → **16C**, the two energy barriers are successively 9.41 and 9.20 kcal/mol. **16C** lies at 14.44 kcal/mol higher than **16A** in the PES. Similar to the cases in **2C** and **4C**, the weakly bonded Al−Li interaction in **16C** can give rise to a relatively easy dissociation (with a PBE0 calculated endothermicity of 10.86 kcal/mol, see reaction 12 in Table 3) from **16C** to a free Li atom and the remnant moiety **16C-li**, whose PBE0 optimized structure is shown in Figure 7. Experiencing the

DOI: 10.1021/acs.jpclett.5b01182
J. Phys. Chem. Lett. 2015, 6, 2950−2958

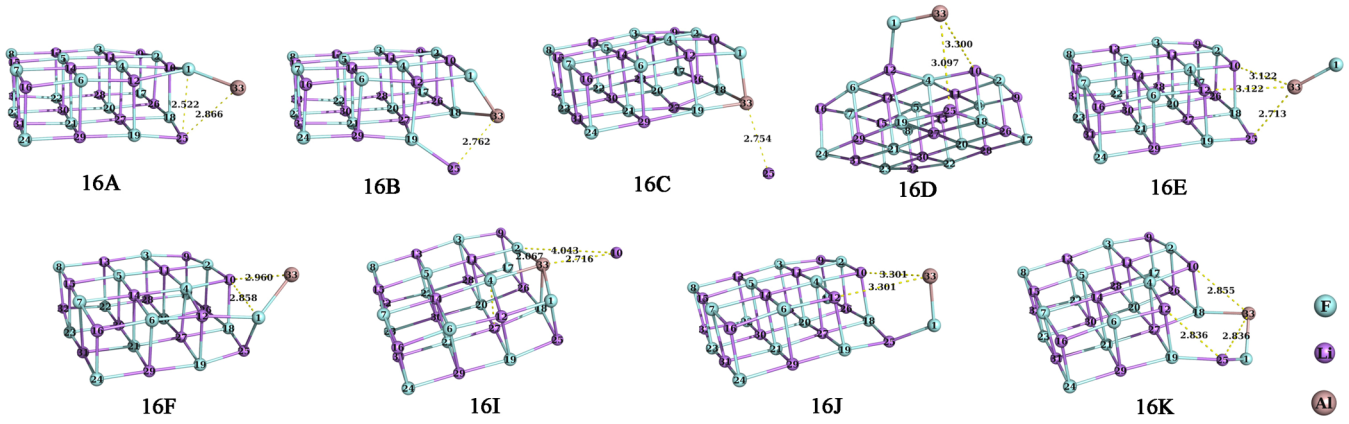

Figure 5. PBE0 optimized minimum structures involved in the Al−$(LiF)_{16}$ system (labeled interatomic distances in Å).

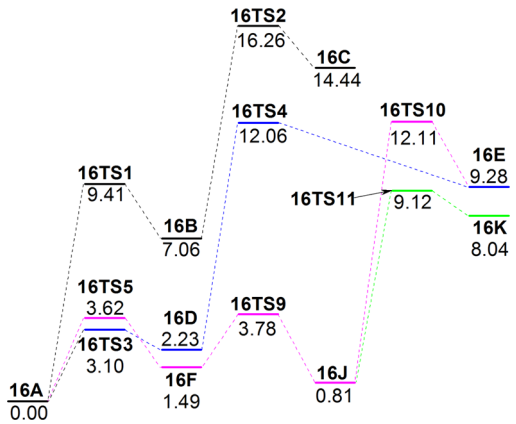

Figure 6. Energy profile for the reactions of the Al−$(LiF)_{16}$ system, with the labeled ZPE-corrected energies (in kcal/mol, calculated by PBE0) relative to **16A**.

Table 3. Calculated Reaction Energies, Δ*E* in kcal/mol, ZPE-Corrected, for the Al−$(LiF)_{16}$ System

reaction	PBE0	M06
Al + 4 × 4 × 2$(LiF)_{16}$ → **16A** (11)	−21.91	−22.03
16C → Li + **16C-li** (12)	10.86	9.75
16E → AlF + **16E-alf** (13)	21.58	21.94
Al + 4 × 4 × 2$(LiF)_{16}$ → **16C-li** + Li (14)	3.39	1.23
Al + 4 × 4 × 2$(LiF)_{16}$ → **16E-alf** + AlF (15)	8.95	11.05

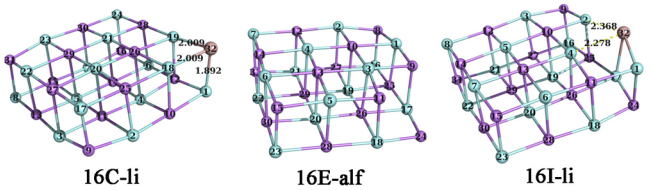

Figure 7. Structures of **16C-li**, **16E-alf**, and **16I-li**.

other two successive energy barriers of 3.10 (across **16TS3**) and 9.83 kcal/mol (across **16TS4**), **16A** can be brought to **16E**, which needs to expend 21.58 kcal/mol (PBE0) energy to dissociate into AlF and the remnant moiety **16E-alf**. Interestingly for the generation of **16E**, there is another pathway **16A** → **16F** → **16J** → **16E**, where the three step energy barriers are 3.62, 2.29, and 11.30 kcal/mol, respectively. From **16J**, **16K** can be generated by overcoming an 8.31 kcal/mol energy barrier, and again similar to **4F**, **16K** has no facile dissociation route found.

Moreover, based on **16F** in which the Al atom is embedded at the long edge rather than at the short edge of 4 × 4 × 2 $(LiF)_{16}$, another structure **16I** with a weakly bonded Li atom has been searched, and the pathway **16F** → **16G** → **16H** → **16I** is shown in Supporting Information Figure S4. However, **16I** is much disfavored by 28.86 kcal/mol relative to **16A** and the remnant moiety (**16I-li** shown in Figure 7) after dissociation is also 16.55 kcal/mol (PBE0) higher than **16C-li** in ZPE-corrected energy, and hence, this pathway is not discussed in the current study.

Reactions 14 and 15 listed in Table 3 are for evaluating the overall processes from Al atom and 4 × 4 × 2 $(LiF)_{16}$ to the dissociated species. The endothermicities of the two processes are close to the corresponding ones in the Al−$(LiF)_4$ system. Both PBE0 and M06 results indicate that the energy compensations are required for the dissociations (reactions 12 and 13) and the overall processes (reactions 14 and 15).

It should be discussed what about the difficulty of the processes of the Li atom coming off from the Al−$(LiF)_n$ systems. The last steps for such processes disscussed in the current study are the dissociations of **2C**, **4C**, and **16C** (reactions 2, 7, and 12), which are only around 10.0 kcal/mol energy endothermic. The endothermicities of these dissociations can be easily offset by the interaction between the released Li atom and mer-Alq_3 (the energy-favored meridianal form of Alq_3). The reported energetics for the interactions of mer-Alq_3−metal are listed in Table 4. The overall replacement reaction 4 is significantly exothermic, and thus the replacement of Al on Li in $(LiF)_2$ is very easy. As for the overall replacements (reactions 9 and 14) in $(LiF)_4$ and $(LiF)_{16}$, the slight endothermicity could be partially compensated by the

Table 4. Calculated Metal-Binding Energies, in kcal/mol, Previously Reported on the Al− or Li−Organic Complexes

	$E_{binding}$	method	reference
mer-Alq_3−Al	37.1	BLYP	ref 58
	42.0	B3LYP	ref 59
mer-Alq_3−Li	39.5	BLYP	ref 58
	42.8	B3LYP	ref 59
benzene−Li	6.7	CCSD(T)	ref 60
pyridine−Li	12.1	B3LYP	ref 61

DOI: 10.1021/acs.jpclett.5b01182
J. Phys. Chem. Lett. 2015, 6, 2950−2958

Table 5. Calculated VIEs, in eV, for the Selected Structures

	2A	2C	2D	4A	4C	4F	16A	16C	16K	2E-alf	4E-alf	16E-alf
PBE0	5.39	4.51	5.83	5.26	3.71	4.74	5.12	3.81	4.56	4.79	4.61	4.47
OVGF	5.16	4.22	5.75	5.07	3.47	4.48	4.96	3.59	4.33	4.51	4.36	4.29

difference between the metal-binding energies of mer-Alq_3−Al (37.1 kcal/mol by BLYP[58] or 42.0 kcal/mol by B3LYP[59]) and mer-Alq_3−Li (39.5 kcal/mol by BLYP[58] or 42.8 kcal/mol by B3LYP[59]). Also, another factor should be taken into account, that is, the released Li atom comes off from the bottom layer of a 2 ML cluster $(LiF)_n$ island where the released Li atom may much more readily reach the binding site of one Alq_3 molecule buried under the cluster island. In **4C** and **16C**, the Al atoms replace the corner Li atoms, and the frontier molecular orbitals (FMOs, showing Al 3p electrons transferred and Al 3s electrons almost undisturbed) and the charges (close to 1.0, vide infra) indicate the +1 valence of the Al atoms. The significant broadening of X-ray photoemission spectroscopy (XPS) Al 2p peak upon Al deposition on LiF/Alq_3 supports the existence possibility of Al(I) at the $Al/LiF/Alq_3$ interface.[15,62]

However, if the underneath layer is not Alq_3 but one organic polymer, such as MEH-PPV,[63] PFO,[27,28] and MDMO-PPV,[29] the Li−organic binding energy (see the reported benzene−Li binding energy listed in Table 4) could not readily offset the endothermic dissociations of **2C**, **4C**, and **16C**. This is consistent with the experimental reports in which the gap state arising at the interfaces $Al/LiF/Alq_3$ and Li/PFO was not evidenced at the interface Al/LiF/PFO.[27,28] Other experimental results based on postpackaging annealing showed that thermal annealing could increase the Li diffuse depth and accordingly significantly enhance the electron injection for Al/LiF/BCP constructed devices but not for $Al/LiF/Alq_3$ constructed ones,[64] which can also be explained by taking into account the difference of Li−organic binding energyies to compete with the barriers and energy changes during the reactions like reactions 12 and 14.

As judged from reactions 3, 8, and 13, it is much more difficult to remove AlF from **2E**, **4E**, or **16E** than to release Li from **2C**, **4C**, or **16C**. Even so, the endothermicities of these dissociation reactions have one approach to be setoff, that is, the disproportionation (reaction 16) of dissociated AlF.[65] The reaction heat (ΔH) of reaction 16 is calculated as −32.8 kcal/mol at 298 K, based on the thermodynamic data of the ref 66. It is worth mentioning that the limited number of AlF_3 molecules might not constitute a perfect bulk phase, and thus the thermodynamic data of AlF_3 in gas phase was used here. Therefore, the overall reaction from the Al−$(LiF)_n$ interacted system to the formation of AlF_3 can be regarded as reaction 17, which is likely exothermic deduced by considering the combination of reactions 15 (or reaction 10) and 16.

$$\mathrm{AlF}(g) \xrightarrow{\Delta H} (1/3)\mathrm{AlF_3}(g) + (2/3)\mathrm{Al}(s) \tag{16}$$

$$\mathrm{Al}(g) + (\mathrm{LiF})_n(s) \rightarrow \mathrm{Li}_n\mathrm{F}_{n-1}(s) + (1/3)\mathrm{AlF_3}(g) + (2/3)\mathrm{Al}(s) \tag{17}$$

Only judging from the exothermicity of reaction 17, we may deduce that the formation reaction of AlF_3 should take place in all Al/LiF interfaces. However, the second ion mass spectroscopy (SIMS) signals of AlF^+ and AlF_2^+ were found with very low intensities at Al/LiF/PCBM or Al/LiF/PPV compared with the corresponding signals of the AlF_3 powder sample.[29] It is worth noticing that the growth mode of the LiF layer probably allows for the deposited islands with large area,[38,67] which effectively limit the number of removable AlF molecules formed at the corners of cluster islands and separate the removable AlF molecules at long distances. Without careful, purposeful and effective controls during processing, the AlF removal reactions (like reactions 10 and 15) and the accordingly overall reaction 17 would occur in very limited amounts. This is different from the releasing processes (like reactions 9 and 14) of free Li atom, where no intermolecular encounter is needed for formations of the final products.

Besides, once reaction 17 occurs, the moieties **2E-alf**, **4E-alf**, and **16E-alf** will be left. And interestingly, these remnant moieties belong to the well-known hyperlithiated compounds containing excess electrons shared by more than one lithium atom.[68−72] The calculated VIE values (listed in Table 5) of **2E-alf** and **4E-alf** are 4.51 and 4.36 eV (OVGF), respectively, which agree with the previously reported values 4.47 eV [CCSD(T,full)] of Li_2F and 4.26 eV (MP2) of Li_4F_3.[72] The larger analogue **16E-alf** has slightly smaller VIE (4.29 eV by OVGF) than **4E-alf**. The calculated VIEs are close to the ionization potentials of the alkali metals K (4.34 eV) and Rb (4.17 eV),[73] suggesting that the excess electrons in these remnant moieties should be loosely bound.

Besides the hyperlithiated compounds **2E-alf**, **4E-alf**, and **16E-alf**, some minima of the Al−$(LiF)_n$ systems were found with low VIEs (see Table 5). Except the calculated VIE values of **2A** and **2D**, all the other OVGF values are lower than the ionization potential of the alkali metal Na (5.14 eV), especially for **4C** (3.47 eV by OVGF) and **16C** (3.59 eV by OVGF), whose OVGF calculated VIEs are explicitly lower than the ionization potential of the alkali metal Cs (3.89 eV).[73] All the PBE0 calculated VIE values are larger than the OVGF ones by around 0.20 eV.

To understand the origins of the low VIEs, it is helpful to visualize the occupied frontier orbitals. The highest singly occupied molecular orbital (SOMO) and SOMO-1 were ploted in Figure 8 for each selected minimum in the Al−$(LiF)_4$ system. The SOMO-1 electrons are from Al 3s atomic orbital, while the SOMO electrons originally arise from Al 3p. In **4A**, SOMO-1 is almost nonbonding, and SOMO is shared between Al and one Li atom (Li5) and accordingly stabilizes the minimum structure as the lowest energy one. In **4C**, the originally nonbonding orbital SOMO-1 accomplishs a donor−acceptor bonding interaction between Al−Li5, while SOMO is almost localized on Li5 and shows a slightly antibonding contribution to Al−Li5, which puts this minimum to a higher energy level. In **4F**, SOMO-1 is also nonbonding, and interestingly, SOMO is delocalized between Al and three Li atoms (Li5, Li6 and Li7). The natural population analysis (NPA)[74] charges definitely indicate the Al 3p electrons are transferred to the atom Li5 and the site above the centroid of Li5, Li6, Li7 and Al9, respectively in **4C** and **4F** (see Table 6). Taking together the frontier orbitals and the NPA charges, it is suggested that the atom Li5 in **4C** should mainly act as a free Li atom and the electron herein should be bound more loosely than in a free Li atom thanks to the minor antibonding

DOI: 10.1021/acs.jpclett.5b01182
J. Phys. Chem. Lett. 2015, 6, 2950−2958

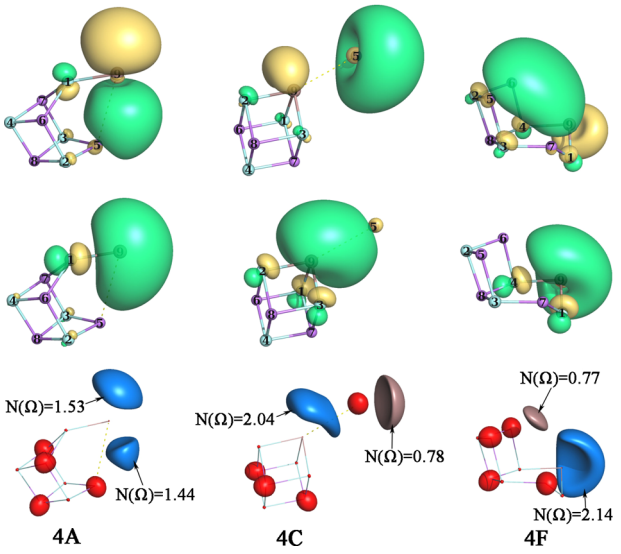

Figure 8. Occupied frontier orbitals (SOMO, top, and SOMO-1, middle, isovalue = 0.035) and ELF = 0.95 isosurfaces (bottom, N(Ω) for basin population) of **4A**, **4C**, and **4F**.

Table 6. Calculated NPA Charges on the Metal Atoms in 4A, 4C, 4F and 16A, 16C, 16K

	4A/16A	4C/16C	4F/16K
Li5/Li25	0.56/0.55	−0.11/−0.07	0.65/0.68
Li6/Li12	0.87/0.82	0.88/0.83	0.55/0.64
Li7/Li10	0.87/0.82	0.88/0.83	0.68/0.52
Li8/Li27	0.88/0.73	0.88/0.69	0.87/0.75
Al9/Al33	0.29/0.32	0.83/0.89	0.73/0.71

contribution in SOMO, pushing the SOMO energy level to −2.314 eV (by PBE0, in comparison to −3.829 eV of the SOMO energy level in the free Li atom). Thus, the VIE of **4C** is extremely low. Meanwhile, **4F** behaves like a so-called electride,[75−79] where an excess electron serves as anion. Also, the electron localization function (ELF)[80,81] analyses (performed with TopMod[82,83]) on the total electron density of **4F** reveal there are 0.77 electrons in the excess electron basin. The analyses on the $(LiF)_{16}$ analogues indicate that **16C** and **16K** possess similar properties to **4C** and **4F**, respectively (see the Supporting Information for details).

Considering the structural relaxations after electron extraction, we optimized the corresponding cation structures. For the Al−$(LiF)_4$ system, the cation structure ($[\mathbf{4F}]^+$ shown in Figure 9) optimized from the **4F** structure is the most stable one, but it experiences large geometrical changes from the **4F** structure and is stretched to a nearly planar geometry. The $[\mathbf{4C}]^+$ structure is very close to the structure of **4C**, and lies a little (1.29 kcal/mol) higher level in energy relative to $[\mathbf{4F}]^+$. Because the slightly antibonding featured **4C** SOMO electron is removed in $[\mathbf{4C}]^+$ and the PBE0 (or M06) calculated energy for the dissociation reaction {$[\mathbf{4C}]^+ \rightarrow Li^+ + \mathbf{4C\text{-}li}$} is 61.2 (or 59.3) kcal/mol, the reason for that $[\mathbf{4C}]^+$ occupies such a low energy site in the cation PES can be attributed to the enhanced Al(I)...Li(I) interaction in the monocation state, where Al(I) acts as a Lewis base.[84] As for the Al−$(LiF)_{16}$ system, unlike the case in the analogue of $[\mathbf{4F}]^+$, the corner of the cation structure $[\mathbf{16K}]^+$ does not experience a large geometrical changes from **16K** due to constraint of the surrounding atoms. Such a situation pushes $[\mathbf{16K}]^+$ to a higher energy level than the cation

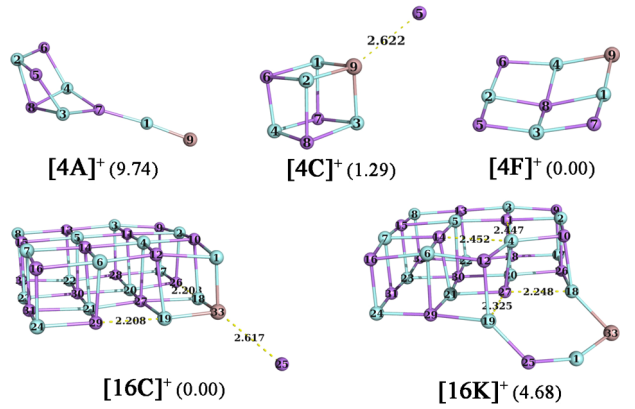

Figure 9. PBE0-optimized cation structures (the values in parentheses for relative ZPE-corrected energies in kcal/mol).

structure $[\mathbf{16C}]^+$ by 4.68 kcal/mol. Also, the optimized cation structure based on $[\mathbf{16A}]^+$ is a (10.74 kcal/mol) higher energy one relative to $[\mathbf{16C}]^+$.

Therefore, after **16A** being taken to **16C** or **16K**, one electron extraction thereat should be considerably easy and will bring about formation of the cation structures $[\mathbf{16C}]^+$ or $[\mathbf{16K}]^+$. In such a way, if no large amount of LiF are considered to dissociate, it could still be explained that the underneath organic molecules were detected as in the anion states.[30,31] Furthermore, we calculated the VEAs of $[\mathbf{16C}]^+$ and $[\mathbf{16K}]^+$ as 2.60 and 2.54 eV (OVGF), respectively. Such extremely low VEAs suggest that these cluster cations should be categorized into superalkali cations[68,85,86] and that the adducts $[\mathbf{16C}]^+e^-$and $[\mathbf{16K}]^+e^-$, likely formed during electron injection in devices, might be regarded as electrides, allowing us to deduce very smooth, fast electron transport through the LiF islands to the underneath organic layers, locally to some extent.[87−89]

DFT investigations on the reaction pathways of the Al−$(LiF)_n$ (n = 2, 4, 16) systems reveal that (i) the Li atom liberating and the formation of AlF_3 are in the two different chemical reaction routes and may not take place at the same time, and the former produce Al(I) rather than Al(III) and the latter leave hyperlithiated clusters Li_nF_{n-1}; (ii) except the process **2A** → **2E** with an energy barrier of 15.46 kcal/mol, the energy barrier of any other reaction step involved in the curruent study is no more than 15.0 kcal/mol, suggesting relative ease for occurrences of these reactions; (iii) even if no dissociation occurs, the Al−$(LiF)_n$ systems have chances to change to some structures with loosely bound electrons, which can facilitate the electron transfers at interface and may shift locally the Fermi level. These findings provided much information about the microscopic chemical changes at the thin LiF interlayer and may be very beneficial to further experimental studies on the issue of OL/electrode interfaces, which is very important in organic electronics applications, for example, OLEDs and OPVCs.

■ ASSOCIATED CONTENT

Supporting Information

The abbreviations, the demonstration on the choice of theoretical methods, all the other involved transition state structures, the energy profile for the reaction pathway from **16F** to **16I**, the FMOs and ELF isosurfaces of the Al−$(LiF)_{16}$ system, and Cartesian coordinates for all optimized structures.

DOI: 10.1021/acs.jpclett.5b01182
J. Phys. Chem. Lett. 2015, 6, 2950−2958

The Supporting Information is available free of charge on the ACS Publications website at DOI: 10.1021/acs.jpclett.5b01182.

AUTHOR INFORMATION

Corresponding Author

*E-mail: zmsu@nenu.edu.cn. Phone: +86 431 85099108. Fax: +86 431 85684009.

Notes

The authors declare no competing financial interest.

ACKNOWLEDGMENTS

The authors gratefully acknowledge financial support from National Natural Science Foundation of China (NSFC 21273030 and 21203020) and SRFDP and RGC ERG Joint Research Program (20120043140001).

REFERENCES

(1) So, F. *Organic Electronics: Materials, Processing, Devices and Applications*, 1st ed.; CRC Press: Boca Raton, FL, 2009.

(2) *Organic Electronics II*; Klauk, H., Ed.; Wiley-VCH: Weinheim, Germany, 2012.

(3) *Physics of Organic Semiconductors*, 2nd ed.; Brütting, W., Adachi, C., Eds.; Wiley-VCH: Weinheim, Germany, 2012.

(4) Gao, Y. Surface Analytical Studies of Interfaces in Organic Semiconductor Devices. *Mater. Sci. Eng., R* **2010**, *68*, 39−87.

(5) Greiner, M. T.; Helander, M. G.; Tang, W.-M.; Wang, Z.-B.; Qiu, J.; Lu, Z.-H. Universal Energy-Level Alignment of Molecules on Metal Oxides. *Nat. Mater.* **2012**, *11*, 76−81.

(6) Turak, A. Interfacial Degradation in Organic Optoelectronics. *RSC Adv.* **2013**, *3*, 6188−6225.

(7) Oehzelt, M.; Koch, N.; Heimel, G. Organic Semiconductor Density of States Controls the Energy Level Alignment at Electrode Interfaces. *Nat. Commun.* **2014**, *5*, 4174.

(8) Hung, L. S.; Tang, C. W.; Mason, M. G. Enhanced Electron Injection in Organic Electroluminescence Devices Using an Al/LiF Electrode. *Appl. Phys. Lett.* **1997**, *70*, 152−154.

(9) Wakimoto, T.; Fukuda, Y.; Nagayama, K.; Yokoi, A.; Nakada, H.; Tsuchida, M. Organic EL Cells Using Alkaline Metal Compounds As Electron Injection Materials. *IEEE Trans. Electron Devices* **1997**, *44*, 1245−1248.

(10) Shaheen, S. E.; Brabec, C. J.; Sariciftci, N. S.; Padinger, F.; Fromherz, T.; Hummelen, J. C. 2.5% Efficient Organic Plastic Solar Cells. *Appl. Phys. Lett.* **2001**, *78*, 841−843.

(11) Brabec, C. J.; Shaheen, S. E.; Winder, C.; Sariciftci, N. S.; Denk, P. Effect of LiF/Metal Electrodes on the Performance of Plastic Solar Cells. *Appl. Phys. Lett.* **2002**, *80*, 1288−1290.

(12) Jabbour, G. E.; Kawabe, Y.; Shaheen, S. E.; Wang, J. F.; Morrell, M. M.; Kippelen, B.; Peyghambarian, N. Highly Efficient and Bright Organic Electroluminescent Devices with an Aluminum Cathode. *Appl. Phys. Lett.* **1997**, *71*, 1762−1764.

(13) Zhang, S. T.; Ding, X. M.; Zhao, J. M.; Shi, H. Z.; He, J.; Xiong, Z. H.; Ding, H. J.; Obbard, E. G.; Zhan, Y. Q.; Huang, W.; et al. Buffer-Layer-Induced Barrier Reduction: Role of Tunneling in Organic Light-Emitting Devices. *Appl. Phys. Lett.* **2004**, *84*, 425−427.

(14) Heil, H.; Steiger, J.; Karg, S.; Gastel, M.; Ortner, H.; von Seggern, H.; Stoßel, M. Mechanisms of Injection Enhancement in Organic Light-Emitting Diodes Through an Al/LiF Electrode. *J. Appl. Phys.* **2001**, *89*, 420−424.

(15) Mason, M. G.; Tang, C. W.; Hung, L.-S.; Raychaudhuri, P.; Madathil, J.; Giesen, D. J.; Yan, L.; Le, Q. T.; Gao, Y.; Lee, S.-T.; et al. Interfacial Chemistry of Alq_3 and LiF with Reactive Metals. *J. Appl. Phys.* **2001**, *89*, 2756−2765.

(16) Hung, L. S.; Zhang, R. Q.; He, P.; Mason, G. Contact Formation of LiF/Al Cathodes in Alq-Based Organic Light-Emitting Diodes. *J. Phys. D: Appl. Phys.* **2002**, *35*, 103−107.

(17) Hill, I. G.; Mäkinen, A. J.; Kafafi, Z. H. Distinguishing between Interface Dipoles and Band Bending at Metal/tris-(8-hydroxyquinoline) Aluminum Interfaces. *Appl. Phys. Lett.* **2000**, *77*, 1825−1827.

(18) Brown, T. M.; Friend, R. H.; Millard, I. S.; Lacey, D. J.; Burroughes, J. H.; Cacialli, F. LiF/Al Cathodes and the Effect of LiF Thickness on the Device Characteristics and Built-in Potential of Polymer Light-Emitting Diodes. *Appl. Phys. Lett.* **2000**, *77*, 3096−3098.

(19) Baldo, M. A.; Forrest, S. R. Interface-Limited Injection in Amorphous Organic Semiconductors. *Phys. Rev. B: Condens. Matter Mater. Phys.* **2001**, *64*, 085201.

(20) Yoon, J.; Kim, J.-J.; Lee, T.-W.; Park, O.-O. Evidence of Band Bending Observed by Electroabsorption Studies in Polymer Light Emitting Device with Ionomer/Al or LiF/Al Cathode. *Appl. Phys. Lett.* **2000**, *76*, 2152−2154.

(21) Ihm, K.; Kang, T.-H.; Kim, K.-J.; Hwang, C.-C.; Park, Y.-J.; Lee, K.-B.; Kim, B.; Jeon, C.-H.; Park, C.-Y.; Kim, K.; et al. Band Bending of LiF/Alq_3 Interface in Organic Light-Emitting Diodes. *Appl. Phys. Lett.* **2003**, *83*, 2949−2951.

(22) Ding, H.; Irfan, F.; Gao, Y. Interface Study of Insertion Layers in Organic Semiconductor Devices. *Proc. SPIE* **2009**, 74150J.

(23) Lee, J.-H.; Kim, J.-J. Interfacial Doping for Efficient Charge Injection in Organic Semiconductors. *Phys. Status Solidi A* **2012**, *209*, 1399−1413.

(24) Wang, H.; Amsalem, P.; Heimel, G.; Salzmann, I.; Koch, N.; Oehzelt, M. Band-Bending in Organic Semiconductors: The Role of Alkali-Halide Interlayers. *Adv. Mater.* **2014**, *26*, 925−930.

(25) Wu, C.-I.; Lee, G.-R.; Pi, T.-W. Energy Structures and Chemical Reactions at the Al/LiF/Alq_3 Interfaces Studied by Synchrotron-Radiation Photoemission Spectroscopy. *Appl. Phys. Lett.* **2005**, *87*, 212108.

(26) Grozea, D.; Turak, A.; Feng, X. D.; Lu, Z. H.; Johnson, D.; Wood, R. Chemical Structure of Al/LiF/Alq Interfaces in Organic Light-Emitting Diodes. *Appl. Phys. Lett.* **2002**, *81*, 3173−3175.

(27) Greczynski, G.; Fahlman, M.; Salaneck, W. R. An Experimental Study of Poly(9,9-dioctyl-fluorene) and Its Interfaces with Li, Al, and LiF. *J. Chem. Phys.* **2000**, *113*, 2407−2412.

(28) Greczynski, G.; Salaneck, W. R.; Fahlman, M. An Experimental Study of Poly(9.9-dioctyl-fluorene) and Its Interfaces with Al, LiF and CsF. *Appl. Surf. Sci.* **2001**, *175−176*, 319−325.

(29) van Gennip, W. J. H.; van Duren, J. K. J.; Thüne, P. C.; Janssen, R. A. J.; Niemantsverdriet, J. W. The Interfaces of Poly(p-phenylene vinylene) and Fullerene Derivatives with Al, LiF, and Al/LiF Studied by Secondary Ion Mass Spectroscopy and X-Ray Photoelectron Spectroscopy: Formation of AlF_3 Disproved. *J. Chem. Phys.* **2002**, *117*, 5031−5035.

(30) Głowacki, E. D.; Marshall, K. L.; Tang, C. W.; Sariciftci, N. S. Doping of Organic Semiconductors Induced by Lithium Fluoride/Aluminum Electrodes Studied by Electron Spin Resonance and Infrared Reflection-Absorption Spectroscopy. *Appl. Phys. Lett.* **2011**, *99*, 043305.

(31) Liu, D.; Nagamori, T.; Yabusaki, M.; Yasuda, T.; Han, L.; Marumoto, K. Dramatic Enhancement of Fullerene Anion Formation in Polymer Solar Cells by Thermal Annealing: Direct Observation by Electron Spin Resonance. *Appl. Phys. Lett.* **2014**, *104*, 243903.

(32) Son, D.; Shimoi, Y.; Marumoto, K. Study on N-Type Doped Electron-Transporting Layers in OLEDs by Electron Spin Resonance. *Mol. Cryst. Liq. Cryst.* **2014**, *599*, 153−156.

(33) Lian, J.-R.; Luo, X.; Chen, W.; Su, S.-X.; Zhao, H.-F.; Liu, S.-Y.; Xu, G.-W.; Niu, F.-F.; Zeng, P.-J. LiF Thickness Dependence of Electron Injection Models for Alq_3/LiF/Al Cathode Structure. *Chin. Phys. Lett.* **2014**, *31*, 118501.

(34) Matsumura, M.; Furukawa, K.; Jinde, Y. Effect of Al/LiF Cathodes on Emission Efficiency of Organic EL Devices. *Thin Solid Films* **1998**, *331*, 96−100.

(35) Anazawa, T.; Tsukada, M.; Kataoka, Y. Charge Injection Spectroscopy of Alq_3 Thin Films Deposited on Bare and LiF-Modified Metal Substrates. *Microelectron. Eng.* **2005**, *81*, 222−228.

(36) Zhu, F.; Low, B.; Zhang, K.; Chua, S. Lithium-fluoride-Modified Indium Tin Oxide Anode for Enhanced Carrier Injection in Phenyl-Substituted Polymer Electroluminescent Devices. *Appl. Phys. Lett.* **2001**, *79*, 1205−1207.
(37) Lee, Y. J.; Li, X.; Kang, D.-Y.; Park, S.-S.; Kim, J.; Choi, J.-W.; Kim, H. Surface Morphology and Interdiffusion of LiF in Alq_3-Based Organic Light-Emitting Devices. *Ultramicroscopy* **2008**, *108*, 1315−1318.
(38) Yokoyama, T.; Yoshimura, D.; Ito, E.; Ishii, H.; Ouchi, Y.; Seki, K. Energy Level Alignment at Alq_3/LiF/Al Interfaces Studied by Electron Spectroscopies: Island Growth of LiF and Size-Dependence of the Electronic Structures. *Jpn. J. Appl. Phys.* **2003**, *42*, 3666−3675.
(39) Adamo, C.; Barone, V. Toward Reliable Density Functional Methods Without Adjustable Parameters: The PBE0 Model. *J. Chem. Phys.* **1999**, *110*, 6158−6170.
(40) Weigend, F.; Ahlrichs, R. Balanced Basis Sets of Split Valence, Triple Zeta Valence and Quadruple Zeta Valence Quality for H to Rn: Design and Assessment of Accuracy. *Phys. Chem. Chem. Phys.* **2005**, *7*, 3297−3305.
(41) Zheng, J.; Xu, X.; Truhlar, D. G. Minimally Augmented Karlsruhe Basis Sets. *Theor. Chem. Acc.* **2011**, *128*, 295−305.
(42) Zhao, Y.; Truhlar, D. G. The M06 Suite of Density Functionals for Main Group Thermochemistry, Thermochemical Kinetics, Noncovalent Interactions, Excited States, and Transition Elements: Two New Functionals and Systematic Testing of Four M06-Class Functionals and 12 Other Functionals. *Theor. Chem. Acc.* **2008**, *120*, 215−241.
(43) Fukui, K. The Path of Chemical Reactions - the IRC Approach. *Acc. Chem. Res.* **1981**, *14*, 363−368.
(44) Hratchian, H. P.; Schlegel, H. B. Using Hessian Updating to Increase the Efficiency of a Hessian Based Predictor-Corrector Reaction Path Following Method. *J. Chem. Theory Comput.* **2005**, *1*, 61−69.
(45) Cederbaum, L. S. One-Body Green's Function for Atoms and Molecules: Theory and Application. *J. Phys. B: At. Mol. Phys.* **1975**, *8*, 290−303.
(46) Zakrzewski, V. G.; von Niessen, W.; Boldyrev, A. I.; Schleyer, P. v. R. Green Function Calculation of Ionization Energies of Hypermetallic Molecules. *Chem. Phys.* **1993**, *174*, 167−176.
(47) Ortiz, J. V. Partial Third-Order Quasiparticle Theory: Comparisons for Closed-Shell Ionization Energies and an Application to the Borazine Photoelectron Spectrum. *J. Chem. Phys.* **1996**, *104*, 7599−7605.
(48) Frisch, M. J., Trucks, G. W., Schlegel, H. B., Scuseria, G. E., Robb, M. A., Cheeseman, J. R., Scalmani, G., Barone, V., Mennucci, B., Petersson, G. A. et al.*Gaussian 09*, Revision D.01; Gaussian, Inc.: Wallingford, CT, 2013.
(49) Eisenstadt, M.; Rothberg, G. M.; Kusch, P. Molecular Composition of Alkali Fluoride Vapors. *J. Chem. Phys.* **1958**, *29*, 797−804.
(50) Berkowitz, J.; Batson, C. H.; Goodman, G. L. PES of Higher Temperature Vapors: Lithium Halide Monomers and Dimers. *J. Chem. Phys.* **1979**, *71*, 2624−2636.
(51) Lintuluoto, M. Theoretical Study on the Structure and Energetics of Alkali Halide Clusters. *J. Mol. Struct.: THEOCHEM* **2001**, *540*, 177−192.
(52) Ochsenfeld, C.; Ahlrichs, R. An Ab Initio Investigation of Structure and Energetics of Clusters K_n Cl_n and Li_nF_n. *Ber. Bunsenges. Phys. Chem.* **1994**, *98*, 34−47.
(53) Fernandez-Lima, F. A.; Vilela Neto, O. P.; Pimentel, A. S.; Ponciano, C. R.; Pacheco, M. A. C.; Chaer Nascimento, M. A.; da Silveira, E. F. A Theoretical and Experimental Study of Positive and Neutral LiF Clusters Produced by Fast Ion Impact on a Polycrystalline LiF Target. *J. Phys. Chem. A* **2009**, *113*, 1813−1821.
(54) Doll, K.; Schön, J. C.; Jansen, M. Ab Initio Energy Landscape of LiF Clusters. *J. Chem. Phys.* **2010**, *133*, 024107.
(55) Haketa, N.; Yokoyama, K.; Tanaka, H.; Kudo, H. Theoretical Study on the Geometric and Electronic Structure of the Lithium-Rich Li_nF_{n-1} (n=2−5) Clusters. *J. Mol. Struct.: THEOCHEM* **2002**, *577*, 55−67.
(56) Al-Sunaidi, A. A.; Sokol, A. A.; Catlow, C. R. A.; Woodley, S. M. Structures of Zinc Oxide Nanoclusters: As Found by Revolutionary Algorithm Techniques. *J. Phys. Chem. C* **2008**, *112*, 18860−18875.
(57) Sangthong, W.; Limtrakul, J.; Illas, F.; Bromley, S. T. Stable Nanoporous Alkali Halide Polymorphs: A First Principles Bottom-up Study. *J. Mater. Chem.* **2008**, *18*, 5871−5879.
(58) Curioni, A.; Andreoni, W. Metal-Alq_3 Complexes:the Nature of the Chemical Bonding. *J. Am. Chem. Soc.* **1999**, *121*, 8216−8220.
(59) Zhang, R. Q.; Lu, W. C.; Lee, C. S.; Hung, L. S.; Lee, S. T. Metal/Alq_3 Interactions in Organic Light Emitting Devices: The Different Roles of Mg, Al, and Li Atoms. *J. Chem. Phys.* **2002**, *116*, 8827−8837.
(60) Denis, P. A.; Iribarne, F. C_{2V} or C_{6V}: Which Is the Most Stable Structure of the Benzene−lithium Complex? *Chem. Phys. Lett.* **2013**, *573*, 15−18.
(61) Krasnokutski, S. A.; Yang, D.-S. High-Resolution Electron Spectroscopy and σ/π Structures of M(pyridine) and M^+(pyridine) (M=Li, Ca, and Sc) complexes. *J. Chem. Phys.* **2009**, *130*, 134313.
(62) Le, Q. T.; Yan, L.; Gao, Y.; Mason, M. G.; Giesen, D. J.; Tang, C. W. Photoemission Study of Aluminum/tris-(8-hydroxyquinoline) Aluminum and Aluminum/LiF/tris-(8-hydroxyquinoline) Aluminum Interfaces. *J. Appl. Phys.* **2000**, *87*, 375−379.
(63) Yang, X.; Mo, Y.; Yang, W.; Yu, G.; Cao, Y. Efficient Polymer Light Emitting Diodes with Metal Fluoride/Al Cathodes. *Appl. Phys. Lett.* **2001**, *79*, 563−565.
(64) Sun, J.; Zhu, X.; Yu, M.; Peng, H.; Wong, M.; Kwok, H. Improving the Performance of Organic Light-Emitting Diodes Containing BCP/LiF/Al by Thermal Annealing. *J. Disp. Technol.* **2006**, *2*, 138−142.
(65) Dohmeier, C.; Loos, D.; Schnöckel, H. Aluminum(I) and Gallium(I) Compounds: Syntheses, Structures, and Reactions. *Angew. Chem., Int. Ed. Engl.* **1996**, *35*, 129−149.
(66) Binnewies, M., Milke, E. *Thermochemical Data of Elements and Compounds*, 2nd ed.; Wiley-VCH: Weinheim, Germany, 2002.
(67) Helander, M. G.; Wang, Z. B.; Mordoukhovski, L.; Lu, Z. H. Comparison of Alq_3/Alkali-Metal Fluoride/Al Cathodes for Organic Electroluminescent Devices. *J. Appl. Phys.* **2008**, *104*, 094510.
(68) Gutsev, G. L.; Boldyrev, A. I. DVM Xα Calculations on the Electronic Structure of "Superalkali" Cations. *Chem. Phys. Lett.* **1982**, *92*, 262−266.
(69) Schleyer, P. v. R.; Wuerthwein, E. U.; Kaufmann, E.; Clark, T.; Pople, J. A. Effectively Hypervalent Molecules. 2. Lithium Carbide (CLi_5), Lithium Carbide (CLi_6), and the Related Effectively Hypervalent First Row Molecules, $CLi_{5-n}H_n$ and $CLi_{6-n}H_n$. *J. Am. Chem. Soc.* **1983**, *105*, 5930−5932.
(70) Rehm, E.; Boldyrev, A. I.; Schleyer, P. v. R. Ab Initio Study of Superalkalis. First Ionization Potentials and Thermodynamic Stability. *Inorg. Chem.* **1992**, *31*, 4834−4842.
(71) Sannigrahi, A. B.; Nandi, P. K.; Schleyer, P. v. R. Ab Initio Theoretical Study of the Electronic Structure, Stability and Bonding of Dialkali Halide Cations. *Chem. Phys. Lett.* **1993**, *204*, 73−79.
(72) Yokoyama, K.; Haketa, N.; Tanaka, H.; Furukawa, K.; Kudo, H. Ionization Energies of Hyperlithiated Li_2F Molecule and Li_nF_{n-1} (n=3,4) clusters. *Chem. Phys. Lett.* **2000**, *330*, 339−346.
(73) Lias, S. G.; Bartmess, J. E.; Liebman, J. F.; Homes, J. L.; Levin, R. D.; Mallard, W. G. Gas-Phase Ion and Neutral Thermochemistry. *J. Phys. Chem. Ref. Data* **1988**, *17*, Supplement 1.
(74) Reed, A. E.; Weinstock, R. B.; Weinhold, F. Natural Population Analysis. *J. Chem. Phys.* **1985**, *83*, 735−746.
(75) Dye, J. L. Electrides: Ionic Salts with Electrons as the Anions. *Science* **1990**, *247*, 663−668.
(76) Dye, J. L. Electrons as Anions. *Science* **2003**, *301*, 607−608.
(77) Dye, J. L. Electrides: Early Examples of Quantum Confinement. *Acc. Chem. Res.* **2009**, *42*, 1564−1572.
(78) Marqués, M.; Ackland, G. J.; Lundegaard, L. F.; Stinton, G.; Nelmes, R. J.; McMahon, M. I.; Contreras-García, J. Potassium Under

DOI: 10.1021/acs.jpclett.5b01182
J. Phys. Chem. Lett. 2015, 6, 2950−2958

Pressure: A Pseudobinary Ionic Compound. *Phys. Rev. Lett.* **2009**, *103*, 115501.
(79) Lee, K.; Kim, S. W.; Toda, Y.; Matsuishi, S.; Hosono, H. Dicalcium Nitride as a Two-Dimensional Electride with an Anionic Electron Layer. *Nature* **2013**, *494*, 336−340.
(80) Becke, A. D.; Edgecombe, K. E. A Simple Measure of Electron Localization in Atomic and Molecular-Systems. *J. Chem. Phys.* **1990**, *92*, 5397−5403.
(81) Silvi, B.; Savin, A. Classification of Chemical-Bonds Based on Topological Analysis of Electron Localization Functions. *Nature* **1994**, *371*, 683−686.
(82) Noury, S., Krokidis, X., Fuster, F., Silvi, B. *TopMod Package*, 1997. http://www.lct.jussieu.fr/pagesperso/silvi/topmod_en.html (accessed May, 2015).
(83) Noury, S.; Krokidis, X.; Fuster, F.; Silvi, B. Computational Tools for the Electron Localization Function Topological Analysis. *Comput. Chem.* **1999**, *23*, 597−604.
(84) Yang, Z.; Ma, X.; Oswald, R. B.; Roesky, H. W.; Zhu, H.; Schulzke, C.; Starke, K.; Baldus, M.; Schmidt, H.-G.; Noltemeyer, M. Janus-Faced Aluminum: A Demonstration of Unique Lewis Acid and Lewis Base Behavior of the Aluminum Atom in $[LAlB(C_6F_5)_3]$. *Angew. Chem., Int. Ed.* **2005**, *44*, 7072−7074.
(85) Tong, J.; Li, Y.; Wu, D.; Wu, Z.-J. Theoretical Study on Polynuclear Superalkali Cations with Various Functional Groups as the Central Core. *Inorg. Chem.* **2012**, *51*, 6081−6088.
(86) Hou, N.; Wu, D.; Li, Y.; Li, Z.-R. Lower the Electron Affinity by Halogenation: An Unusual Strategy to Design Superalkali Cations. *J. Am. Chem. Soc.* **2014**, *136*, 2921−2927.
(87) Miyakawa, M.; Kim, S. W.; Hirano, M.; Kohama, Y.; Kawaji, H.; Atake, T.; Ikegami, H.; Kono, K.; Hosono, H. Superconductivity in an Inorganic Electride $12CaO{\cdot}7Al_2O_3{:}e^-$. *J. Am. Chem. Soc.* **2007**, *129*, 7270−7271.
(88) Toda, Y.; Yanagi, H.; Ikenaga, E.; Kim, J.; Kobata, M.; Ueda, S.; Kamiya, T.; Hirano, M.; Kobayashi, K.; Hosono, H. Work Function of a Room-Temperature, Stable Electride $[Ca_{24}Al_{28}O_{64}]^{4+}(e^-)_4$. *Adv. Mater.* **2007**, *19*, 3564−3569.
(89) Yanagi, H.; Kuroda, T.; Kim, K.-B.; Toda, Y.; Kamiya, T.; Hosono, H. Electron Injection Barriers between Air-Stable Electride with Low Work Function, C12A7:e^-, and Pentacene, C_{60} and Copper Phthalocyanine. *J. Mater. Chem.* **2012**, *22*, 4278−4281.

DOI: 10.1021/acs.jpclett.5b01182
J. Phys. Chem. Lett. 2015, 6, 2950−2958